Link sito dell'editore: https://journals.sagepub.com/doi/10.1177/0954410018811196

Link codice DOI: 10.1177/0954410018811196

Citazione bibliografica dell'articolo:

Giulio Avanzini, David S. Martinez, "Risk Assessment in Mission Planning of Uninhabited Aerial Vehicles", Proceedings of the Institution of Mechanical Engineers, Part G: Journal of Aerospace Engineering, Vol. 233, No. 10, Ago. 2019, pp. 3499-3518

Risk Assessment in Mission Planning of Uninhabited Aerial Vehicles

Giulio Avanzini,[1] and David S. Martínez[1]

Abstract

A procedure for evaluating the risk related to the use of Unmanned Aerial Systems over populated areas is proposed. A nominal trajectory, planned for performing a given mission, is represented by means of motion primitives, that is, segments and arcs flown in a steady state condition. The risk of hitting a person on the ground after catastrophic failure is evaluated as a function of vehicle reliability and population density (assumed known), and position of the impact point (which depends on initial conditions at the time of failure and trajectory flown afterwards). In the deterministic case, a lethal area is introduced and the risk at each point on the ground is proportional to the amount of time spent by the point inside the lethal area. Under the assumptions of a ballistic fall, the position of the lethal area with respect to the nominal trajectory depends only on altitude and velocity at the time of failure. When the effect of navigation errors is introduced, impact points are described by a statistical impact footprint, assuming that position and velocity errors at time of failure are normally distributed with known standard deviations. The two approaches are compared for a fictitious, yet realistic, mission scenario.

Keywords

Uninhabited Aerial Vehicles/Systems, Mission planning, Risk assessment, Lethal area, Motion primitives

Introduction

The paper aims at providing a method for evaluating the risk related to flying a prescribed flight path over a populated area, assuming that population density is known. The use of Unmanned Aerial Systems (UASs) is nowadays well established

[1] Department of Engineering for Innovation (DII), Università del Salento, Lecce, Italy

Corresponding author:
Giulio Avanzini, Università del Salento, Department of Engineering for Innovation, Via per Monteroni, 73100 Lecce, Italy.
Email: giulio.avanzini@unisalento.it

in many military applications[1–4], but use on the battleground or in restricted areas unaccessible to the public clearly makes safety a less critical aspect in managing the whole mission profile. Conversely, the increasing interest for the use of UASs in diverse civil applications clearly requires the definition of precise rules and procedures for safely managing UAS missions in the civil airspace, where conventional aircraft may also be present and part of the mission may involve flight over populated areas. The definition of procedures for the identification of liability in case an accident occurs is another issue at stake, for allowing the use of UAS over populated areas.

For these reasons, a debate is taking place among potential users and companies which design, build and sell UAS over a wide range of size and configurations, on one side, and airspace regulatory authorities on the other one. The first releases of rules for the use of UAS in the civil airspace are being developed and both the industrial and the academic communities are providing contributions to the debate, in order to guarantee safety without harming the profitability of a potentially huge market for UASs.[5]

An accurate and reliable assessment of the risk implied by the use of remotely piloted and/or unmanned autonomous aerial vehicles (RPVs and UAVs) in the civil airspace over populated areas is one of the key-points in the definition of regulations and mission planning strategies for this class of vehicles. One of the crucial aspects for this assessment is the correlation between diverse statistical data, namely, vehicle reliability, guidance accuracy along the prescribed trajectory, environmental conditions (in particular wind and turbulence levels) and population density.

During the last twenty years several studies have approached the problem of evaluating the risk for the population due to ground impact of UAVs. Most of them are based on the concept of lethal area, defined as a function of aircraft size and impact velocity, assuming fatal injuries for all people within that area.[6–9]

This over-conservative approach was improved by Weibel *et al.*,[1;10] who performed a hazard analysis for different types of UAVs and operations, introducing a penetration factor, which accounts for a lower risk posed by smaller UAVs and protection offered by obstacles in the crash area. Weibel and his co-workers modeled the exposure effect using a debris-footprint based model – which is different from the lethal area introduced above – for identifying the area on the ground where the risk of being hit is significant. The study proves that ground impact risk varies significantly, depending on population density, and increasing with vehicle kinetic energy. The expected number of people exposed to harm was defined as the product of the area of exposure and the population density of the area, ρ, expressed in terms of number of people per unit area. All the risk-mitigating circumstances were included in a mitigation factor, which represents the probability that a ground fatality does not occur because of effects such as sheltering.

Dalamagkidis *et al.*[2] presented a simple (but once again rather conservative) method to calculate the probability of fatalities and the fatality rates associated with a ground impact based on UAV type, population density and sheltering factor, similar to the penetration factor introduced by Weibel[1]. The sheltering factor accounts for the fact that not all the impact energy arrives to a person, but it is mitigated by obstacles such as trees, buildings or cars. However, the impact area was calculated in a deterministic way, following the definition of lethal area.

In light of the available studies, it may be possible to safely operate small UAVs (such as those classified as micro- or mini-UAVs) in the public airspace, away from

only the most densely populated areas. For instance, Weibel *et al.*[1] established that a mean time between failures as high as 100 hours is necessary for reaching a target level of safety equal to $1{\cdot}10^{-8}$ fatalities per hour of operation. However no method is proposed to determine the value of the penetration factor, which significantly affects the risk estimate. Moreover, either the definition of lethal area or the employment of debris-footprint do not take into account the influence of navigation errors on the location of impact on the ground, which can lead to underestimate the hazard areas.

The work by Lum *et al.*[11] summarizes the various approaches listed above, combining concepts such as lethal area, distribution of population density and probability of catastrophic failure. A fixed wing UAV model was considered in numerical simulations aimed at determining the impact point when failure occurred at different operating conditions. A probability density function (PDF) for impact points was empirically determined in terms of polynomial fitting first, and then approximated by a normal distribution. The PDFs were combined with population density maps to establish the level of risk. The authors determined the shape of the PDFs for both glide angle and crash distance as a function of the flight condition at the moment of failure, which significantly affects them. It is then clear that navigation errors represent an issue, when determining the hazard area, provided that actual operating conditions at the time of failure may be different from those expected for the nominal trajectory.

The present paper aims at providing a contribution towards the definition of a reliable, yet numerically efficient, combined procedure for path planning and risk evaluation in the framework of mini- and micro-UAS missions over populated areas. The procedure is based on a few assumptions. First of all, the area where the mission is being planned is divided into squares, inside which population density is assumed known and uniform. A reliability factor (expressed in terms of number of catastrophic failures N per flight hour) for the considered vehicle is also assumed known. As a consequence, given the total flight time T (expressed in hours) for the considered mission, the probability of a failure becomes equal to $P_F = NT \times 100\%$. The flight condition in terms of airspeed and altitude along the nominal flight path, together with the physical characteristics of the vehicle, determines the so-called lethal area, that is, the portion of the ground surface where the potential impact of the vehicle may results into a casualty. The lethal area takes into account the final glide angle prior to impact and the effect of debris dispersion due to fragmentation of the vehicle upon impact, which depends on the kinetic energy of the vehicle at impact, and, possibly, explosion due to the presence of detonating material.

In what follows, and for the sake of simplicity, no sheltering or penetration factor will be considered, provided the procedures for the determination of these factors are out of the scopes of the present paper. Nonetheless one should note that, once the operational area is discretized, it is possible to attribute to each square element an average sheltering factor, which represents the percentage of the population of the square assumed to be inside buildings or vehicles, and as such, protected from impact with the falling vehicle or debris. This means that, by means of an *ad hoc* analysis of how the population is expected to be distributed in the area, the procedure can be applied in the very same way, including the sheltering factor, once determined. Thus, even though sheltering represents a significant risk mitigating factor for the outcome of the risk analysis procedure, its inclusion in the analysis does not affect the numerical

procedure, when the population density of each square, which will be used in the sequel, is substituted by an expected number of exposed persons per unit area.

Similarly, the vehicle reliability factor is assumed uniform along the trajectory, which is another simplifying assumption, provided accidents occur more frequently during flight terminal phases, at takeoff and/or landing/recovery of the vehicle. On one side, terminal phases usually cover a minor portion of the planned trajectory, and usually their contribution to the overall risk to third parties can be expected to be minor. As an alternative, it is possible to assume that terminal phases always occur in segregated areas, not accessible to third parties, thus providing no contribution at all to the overall risk. A uniform distribution of accident risk along the planned mission trajectory thus becomes an acceptable assumption, which alleviates the numerical and statistical difficulties of the risk analysis, which would otherwise require a more stringent distinction between different vehicle flight regimes.

Under the simplifying assumptions discussed above, the probability of damage to humans on the ground when the aircraft is flying the nominal trajectory can be estimated from the population density at each point of potential ground impact multiplied by the time spent by each point on the ground surface inside the lethal area. The dispersion of the impact points due to navigation errors on the size of the area where the impact is likely to happen is then included in the statistical model. A Monte Carlo analysis is performed for the determination of the standard deviations σ_x and σ_y, which represents the deviations of the impact point in the along-track and cross-track directions, respectively, with respect to the (deterministic) one obtained for a ballistic trajectory from the nominal point on the planned route. The result is to widen the area of potential impact, but reduce the probability of the impact at each given point.

In the present analysis, the dispersion is determined as a function of navigation errors on vehicle position and velocity at time of failure, assuming that the vehicle falls along an approximately ballistic trajectory after failure. This latter assumption reasonably holds for rotary-wing vehicles only. In the case of winged vehicles, the possibility of (potentially long) glides, strongly affected by wind and turbulence, makes the statistical analysis of impact points more difficult and dependent on unpredictable environmental conditions at the time the mission is actually carried out. The impact footprint is expected to become significantly wider, especially when the glide starts at higher altitude, thus exposing a larger number of people to a potential danger. The statistical distribution of impact points after a glide in turbulent air is thus the object of on-going research.

Nonetheless one should note that, in principle, once the statistical distribution of impact points with respect to the nominal impact after a glide starting from the failure point becomes known, all the fundamental aspects of the analysis proposed in what follows remain once again virtually unchanged. In case a flight termination system is present, which produces fragmentation of the vehicle, the analysis performed in the present paper holds for each one of the major non-lifting elements of the vehicle, after fragmentation. If an aerodynamic deceleration system (i.e. a parachute) is present, the analysis will be performed as for the gliding vehicle.

The risk analysis is performed after dividing the trajectory into a finite number M of elements, each one associated to a motion primitive, that is, each element is represented by a segment or an arc flown in a steady state condition in rectilinear, turning and/or

climbing flight. This approach, borrowed and adapted from the robotic literature,[12] allows for describing each motion primitive by means of a small number of parameters. In the case of a flying vehicle, only four parameters are sufficient, namely airspeed, V, climb rate, $\dot{h}$ (or, equivalently, climb angle γ), turn rate $\dot{\chi}$, and time required to fly the arc Δt (or equivalently its length s), where h and χ are altitude and heading angle, respectively. Given initial values for vehicle position, $\mathbf{r}_0 = (x_0, y_0, -h_0)$ in the local vertical – local horizontal reference frame fixed with respect to the ground, and heading angle, χ_0, the whole trajectory is then described, by means of $4M + 4$ parameters, thus making motion planning very efficient. The use of motion primitives also easily allows for enforcing feasibility constraints on each element in terms of admissible values for required power, load factor and lift coefficient (for fixed wing aircraft). Transient manoeuvres for passing from one steady state to a different one are neglected.

Under the assumption of a ballistic fall, the position of the nominal impact point and the statistical impact footprint only depend on altitude, velocity and climb rate at the time of failure, that is, on only two of the parameters which describe the motion primitives (V and $\dot{h}$) plus altitude (h). The position of the impact point and the impact footprint can thus be determined once, spanning the admissible values of the parameters, and then applied to the planned trajectory as required. Thus, the statistical analysis for the statistical impact footprint can be performed only once, and then be applied to the particular trajectory considered, without the need for time-consuming and computationally demanding Monte Carlo simulations of the whole mission.

In the next paragraph, the representation of the whole trajectory in terms of motion primitives is described, together with the data necessary for planning the mission. The effect of motion parameters on deterministic and statistical lethal areas is then assessed, as discussed above. The risk associated to each segment is thus evaluated as a function of the values of the parameters which describe the corresponding motion primitive, determining size and position of the lethal area or of the statistical impact footprint. The total risk is obtained by numerically integrating the risk along each element, as described in Section 4, and summing up the results for all the M elements. The whole procedure is described in Section 5, where a representative example is analysed by means of the two approaches. A section of conclusions ends the paper.

Mission planning

Representation of Vehicle Trajectory

Motion Primitives For the sake of simplicity, Earth curvature will be here neglected, assuming UAS operations take place over a limited area. A local vertical – local horizontal topocentric frame $\mathcal{F}_I$, fixed with respect to the ground, is assumed as an acceptable approximation of an inertial frame, when Earth curvature and rotation are neglected. If no peculiar aspect of the mission requires a different choice, a North-East-Down (NED) axis triad can be chosen, where the vertical z–axis is parallel to the gravity acceleration vector (local vertical), the x–axis points towards North and the y–axis points towards East, completing a right-handed triad. As a consequence of this choice, the altitude of the vehicle above the local horizontal plane is equal to $h = -z$.

The altitude above the ground is equal to $h_G = h - H(x, y)$, where H represents the elevation of ground and/or obstacles above the horizontal plane.

Steady state conditions for a vehicle flying over a flat, non-rotating Earth are (possibly degenerate) helicoidal trajectories.[13] This means that, when flying at steady state, an aircraft follows either a rectilinear flight path with constant velocity and (possibly zero) climb rate or an arc of an helix (which degenerates into an arc of a circle, when the climb rate is zero), with constant speed and turn rate. A total of three parameters are thus sufficient for describing the geometry of the trajectory flown at steady state, namely flight speed V, climb rate $\dot{h} = V \sin\gamma$ (or equivalently climb angle, γ), and turn rate $\dot{\chi}$. When $\dot{\chi} = 0$, a steady rectilinear flight trajectory is considered. When $\dot{h} = 0$, a level flight condition is dealt with. A hovering condition for rotorcraft can also be considered, with $V = 0$, in which case climb and heading angles γ and χ become undetermined.

A motion primitive is a portion of a trajectory flown at steady state. A fourth parameter is required for completing the description of the primitive arc or segment, namely the time Δt required for flying it or, equivalently, its length $\Delta s = V\Delta t$. For operations over wider areas, which require to account for Earths curvature, a transformation in terms of longitude, latitude, and altitude is easily achieved. Also note that, when operating in a subsonic speed regime, as most current state-of-the-art UAS, effects of Earth's rotation remain negligible.

It is possible to divide a mission trajectory into a finite number M of motion primitives, assuming that the time required for passing from one steady state condition to a different one is sufficiently small with respect to Δt_k, $k = 1, 2, \ldots, M$. Vehicle position at time t, for $t_{k-1} < t \leq t_k$ (where $\Delta t_k = t_k - t_{k-1}$) is thus known as a function of the values of V_k, $\dot{h}_k$ and $\dot{\chi}_k$ and initial position $\mathbf{r}_{k-1}$ and direction of the velocity vector, χ_{k-1}, at time t_{k-1}. The increment of the position vector $\Delta\mathbf{r}(t)$ for $t_{k-1} < t \leq t_k$ is given by

$$\Delta\mathbf{r}(t) = (\Delta x(t), \Delta y(t), \Delta z(t))^T$$

where, regardless of the value of $\dot{\chi}_k$, one has that

$$\Delta h(t) = -\Delta z(t) = \dot{h}_k(t - t_{k_1})$$

When $\dot{\chi}_k = 0$, a rectilinear primitive is considered and $\Delta\chi_k = 0$ (which implies that $\chi_k \equiv \chi_{k-1}$), whereas trajectory curvature vanishes, that is, $1/R = 0$. In this case it is

$$\begin{aligned} \Delta x(t) &= [V_k \cos\gamma_k \cos\chi_k]\,(t - t_k) \\ \Delta y(t) &= [V_k \cos\gamma_k \sin\chi_k]\,(t - t_k) \end{aligned}$$

At time $t = t_k$ one gets

$$\Delta x_k = \Delta x(t_k) = V_k\,\Delta t_k \cos\gamma_k \cos\chi_k \quad (1)$$

$$\Delta y_k = \Delta y(t_k) = V_k\,\Delta t_k \cos\gamma_k \sin\chi_k \quad (2)$$

For a turning flight segment ($\dot{\chi}_k \neq 0$) the total variation of the heading angle is $\Delta\chi_k = \dot{\chi}_k\Delta t_k$, where a positive value of $\dot{\chi}_k$ indicates a right turn, whereas a negative

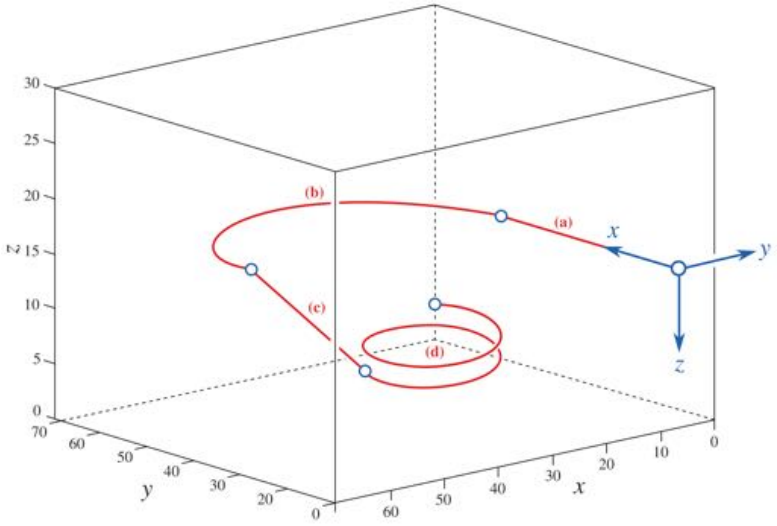

Figure 1. Example of different flight motion primitives: (a) straight horizontal; (b) turn in the horizontal plane; (c) straight descent; (d) climbing turn.

value indicates a left turn. For a constant flightpath curvature radius $R = V_k \cos\gamma_k / \dot{\chi}_k$, the increments of the position vector components in the horizontal plane are equal to

$$\begin{aligned} \Delta x(t) &= R\,\sin[\dot{\chi}_k(t-t_k)]\cos\chi_{k-1} - R\,\mathrm{sign}\dot{\chi}_k\{1-\cos[\dot{\chi}_k(t-t_k)]\}\sin\chi_{k-1} \\ \Delta y(t) &= R\,\sin[\dot{\chi}_k(t-t_k)]\sin\chi_{k-1} + R\,\mathrm{sign}\dot{\chi}_k\{1-\cos[\dot{\chi}_k(t-t_k)]\}\cos\chi_{k-1} \end{aligned}$$

The total position vector increment in the horizontal plane at time t_k is thus equal to

$$\Delta x_k = \Delta x(t_k) = R\,[\sin\Delta\chi_k\cos\chi_{k-1} - \mathrm{sign}\dot{\chi}_k\,(1-\cos\Delta\chi_k)\sin\chi_{k-1}] \quad (3)$$

$$\Delta y_k = \Delta y(t_k) = R\,[\sin\Delta\chi_k\sin\chi_{k-1} + \mathrm{sign}\dot{\chi}_k\,(1-\cos\Delta\chi_k)\cos\chi_{k-1}] \quad (4)$$

The whole trajectory is thus described by means of $4M+4$ parameters, namely 4 values for velocity, climb rate, turn rate and duration of each motion primitive arc or segment plus 3 coordinates for the initial position and the initial heading angle at time t_0. An example for $M = 4$ is reported in Fig. 1, where an initial steady rectilinear level flight segment (a) is followed by a 180 deg turn (b), a rectilinear descent (c) followed by a climbing spiral (d).

Performance Limitations One of the advantages in the use of motion primitives is that it is relatively easy to enforce feasibility constraints on the elements that constitute the planned trajectory. This is a relevant difference with respect to other trajectory planning techniques, where performance limitations need to be evaluated at each point of the trajectory, as it happens when using spline interpolants.[14] Conversely, all performance parameters are constant along each motion primitive and they can be estimated from the kinematic data describing it. For a fixed wing aircraft weighting W, with a wing

surface S and a parabolic drag polar $C_D = C_{D_0} + KC_L^2$ (where C_L and C_D are lift and drag aerodynamic coefficients, respectively, C_{D_0} being the parasite drag coefficient and K the induced drag factor), load factor, lift coefficient and necessary power along the k–th primitive arc or segment are respectively equal to [15]

$$(n_z)_k = 1 + (V_k \dot{\chi}_k / g)^2 \quad (5)$$

$$(C_L)_k = (n_z)_k (W/S)/(0.5\rho V_k^2) \quad (6)$$

$$(P_n)_k = 0.5\rho V_k^2 S C_{D_0} + 2KW^2/(\rho V_k^2 S) + W\dot{h}_k \quad (7)$$

where ρ is air density at flight altitude.

Data such as aerodynamic drag polar and maximum lift coefficients, maximum structural load factor and maximum engine power or thrust are usually known from the aircraft manufacturer or estimated early in the design process. A trajectory is feasible if the values of n_z, C_L and P_n, which are all constant along a motion primitive element, satisfy performance limitation constraints, that is,

$$(n_z)_k \leq n_{z_{\max}} \ , \ \ (C_L)_k \leq C_{L_{\max}} \ , \ \ (P_n)_k \leq P_{d_{\max}}$$

For rotorcraft, the major performance limitation is provided by available engine power (and/or battery power for small-scale electrically powered platforms), which needs to remain higher than required power along the considered motion primitive, in order to make it feasible. The expression of required power at steady state can also be calculated on the basis of the kinematic informations which describe the primitive arc or segment, [15] but the procedure and the corresponding equations, summarized in some detail in [16], are more cumbersome and they are omitted here for the sake of conciseness.

Mission scenario

Map and obstacles A trajectory planning method requires the a priori knowledge of the operational area in terms of orographic characteristics, buildings and obstacles. In what follows, it is assumed that a map is available, which provides all the relevant information for planning a trajectory. By sampling the planned trajectory with a sufficiently fine space resolution, it is possible to guarantee that the altitude of the vehicle never falls below a safety margin above ground level. At the same time, minimum distance from obstacles can be evaluated and maintained above a prescribed safety threshold. All these aspects are nowadays common practice in trajectory planning algorithms. Their implementation is not discussed here, being out of the scopes of the paper. A fictitious map was realized for the present study, which features all the critical elements of a coastal urban environment.

Population density The risk assessment procedure, as outlined in the Introduction, requires that, together with the physical characteristics of the operational area, also the distribution of population is known. In the present paper, it is assumed that this information is available on a discrete square grid. Population is assumed uniformly distributed inside each grid element.

Several aspects make the generation of these data far from trivial. First of all, population density is a dynamic feature of the area of operations, provided that different

areas can be more or less densely populated, depending on the time of the day (schools, houses and offices move large portions of the population in an urban environment), day of the week (population distribution on weekends is different from that of a working day) and even season (*e.g.* a shore can be densely crowded in summer and almost desert in winter). Also, unpredictable events can change the population distribution (*e.g.* a car accident which slows traffic and generates a crowd).

Long term mission planning (*i.e.* planning a mission much time in advance or planning a mission which requires several flight hours) can be based only on average conditions estimated from a combination of satellite pictures and *in situ* observations. In this respect, a conservative risk estimate should be based on a reduced value of the sheltering factor.

In the present work, a realistic but fictitious operation area will be considered, where the population distribution on the discrete grid will be assumed constant. Relatively short trajectories will be considered for the implementation of the deterministic and statistic risk evaluation methodologies, which do not require including the dynamic variation of population density with time. This aspect do not affect the general validity of the approach to more complex operative scenarios, where population densities and possibly sheltering factor are known functions of time.

Risk Assessment

General Principles

In general terms, the elements that contribute to the risk related to UAS operations over a populated area are

1. probability of an uncontrolled/catastrophic failure, inversely proportional to vehicle reliability, quantified by means of a failure rate per unit time, p_F;
2. probability of impact on a given area, p_I;
3. size of the impact area, which depends on size of the vehicle, glide angle and kinetic energy at time of failure and at impact , A_ℓ;
4. density of the population in the impact area, ρ.

In mathematical terms, the risk R is given by

$$R = p_F \cdot p_I \cdot A_\ell \cdot \rho$$

As stated in the Introduction, the objective of the paper is to provide a tool that allows for assessing the risk R for a generic trajectory, as qualitatively depicted in Fig. 2. In order to reduce the risk of collision and casualties when flying from point labeled ‘Start’ to point labeled ‘End’, it is necessary to circumvent obstacles, while keeping the trajectory away from more densely populated areas.

The reliability of the vehicle depends on how the vehicle is designed and manufactured. The value can be determined on the basis of well assessed methodologies, such as Fault Tree Analysis (FTA)[17] or Failure Mode, Effects, and Criticality Analysis (FMECA).[18] The probability p_F is assumed constant over the entire trajectory. This is clearly a simplifying assumptions, provided that failures may depend on how severe structure and propulsion system are being challenged during

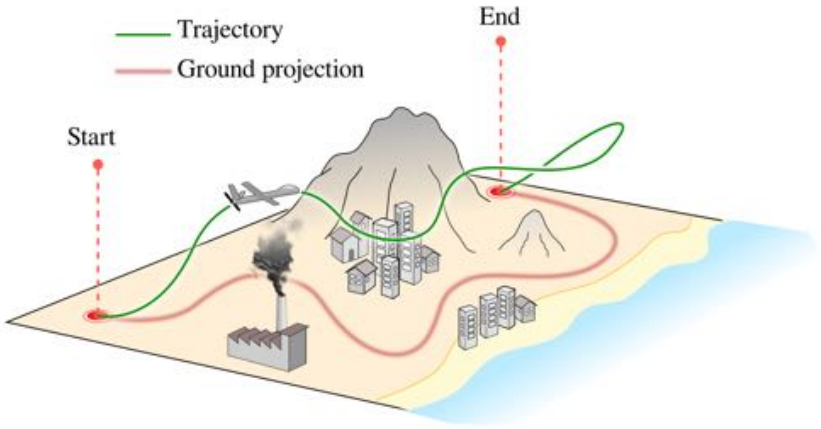

Figure 2. Illustrative example of a flight trajectory and its ground track in an inhabited area.

the considered maneuvers, especially during flight terminal phases. Nonetheless, when the vehicle is performing flying tasks well inside its design maneuver envelope, the assumptions is reasonable and realistic. Takeoff and landing are assumed to take place in restricted area, thus not contributing to overall risk against third parties. The determination of p_F is out of the scopes of the present papers and its value is assumed known from external sources (manufacturer, users, past experience, etc.). Its value clearly affects the final result of the risk analysis, but not the risk assessment procedure.

The density of the population is assumed known and constant over a finite size area element. Also this set of data comes from external sources. In the application example, population density is provided over a regular square grid, formed by elements of size equal to 100×100 m. The focus is now shifted on the other two elements of the product, namely p_I and A_ℓ, the value of which depend on the type of approach adopted for identifying the potential collision with a person standing on the ground in the impact area.

Deterministic Approach

The deterministic lethal area (DLA) is the area within which a person on the ground can be hit and, possibly, seriously injured by an unmanned aerial vehicle crashing on the ground. The DLA can be evaluated on the basis of the sketch represented in Fig. 3, taken from Ref. 19, where the size of a person is approximated by means of a cylinder of height h_P and radius r_P. Letting b be the width of the vehicle and γ its glide-path angle when crashing on the ground, the size of the impact area is assumed to be a circle of radius $b/2$. A person can be hit (i) if he/she is on the final segment of the trajectory, the length of which is $d = h_P / \tan\gamma$, when projected on the ground (Fig. 3.a), (ii) if he/she is hit by the vehicle skidding on the ground after impact, or (iii) by debris after a possible explosion and/or fragmentation of the vehicle.

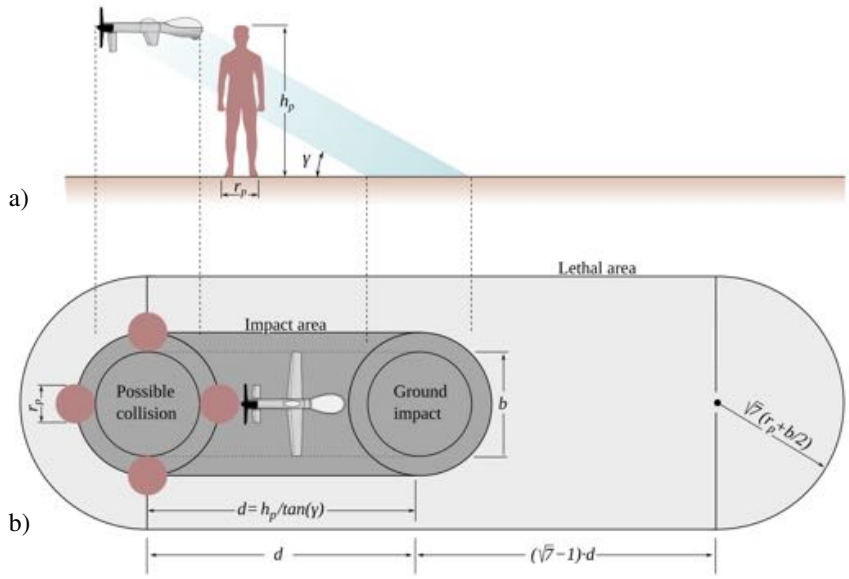

Figure 3. Sketch for the determination of the deterministic lethal area: side (a) and top (b) views of the different geometries.

The DLA is build by joining a rectangle of length d and width $b + r_P$ with two half circles of diameter $b + r_P$. Its area is then incremented by a factor 7, for taking into account skidding after impact. Hence all dimensions are increased by a factor $\sqrt{7}$, where the increase in length, $(\sqrt{7} - 1)d$, is placed after the expected impact point, as shown in Fig. 3.b. A further multiplicative factor k can be added, for accounting the effect of debris around the impact area.[19] This coefficient can be varied, depending on the presence of inflammable or explosive materials on board, but it will not be considered in the analysis discussed in what follows.

In the deterministic case, the position of the center of the impact circle and the glide path angle at impact are determined by vehicle velocity and height above the ground at the time of the catastrophic failure, if one assumes that the trajectory after failure is parabolic. The probability of hitting a person lying inside the DLA is $p_I = 1$, if the person is in the open air. A sheltering factor, if known, can be introduced at this level, reducing p_I by a factor $(1 - p_S)$, where p_S is the fraction of the population of the grid element expected to be protected by features of the landscape or inside vehicles and buildings. The determination of a sheltering factor is out of the scopes of the paper. Hence $p_I = 1$ is assumed, for the sake of simplicity.

If the population density is described by a grid density map, the risk R defined above associated to a cell i of the map can be expressed as

$$R_i = p_F \cdot A_\ell \cdot (t_i/t_M) \cdot \rho_i$$

where A_ℓ is the lethal area associated to the flight condition (height and velocity), t_i is the time spent by the DLA inside the i–th cell, and t_M is the total mission time.

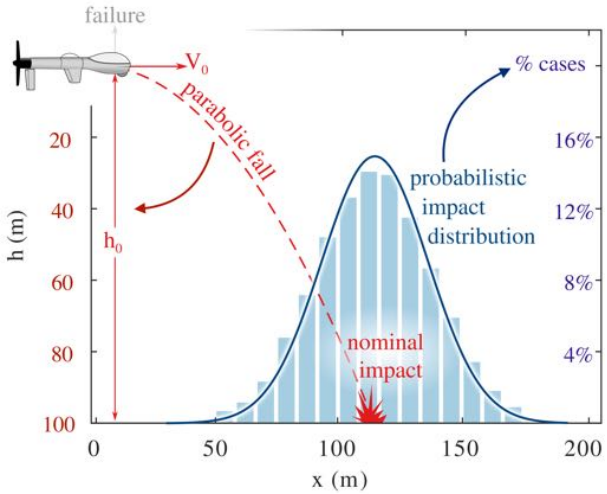

Figure 4. Statistic impact footprint for parabolic trajectories (illustrative 2-D example)

Statistic Approach

Principles of the Statistical Analysis As a major approximation, the evaluation of the risk related to a given flight trajectory by means of the DLA is performed under the assumption that, at any time instant, position and velocity of the vehicle along the trajectory are those prescribed for the considered mission phase. As a matter of fact, the actual trajectory flown by the RPV/UAS will differ from the planned one. Navigation errors will be present in executing the considered mission task, the size of which is related to atmospheric disturbances, performance of the guidance, navigation and control (GNC) system and/or ability of the remote pilot (depending on the degree of autonomy of the vehicle).

The uncertainty on the actual position and velocity at the time of catastrophic failure can be taken into consideration by assuming that initial position and velocity vector components are randomly distributed around their nominal values for the planned trajectory. Assuming a parabolic trajectory, as in the previous case, it is possible to determine the nominal impact point. The actual impact point will be randomly distributed around the nominal one with a probability density function which depends on the statistical distribution of navigation errors. The statistical impact footprint (SIF) is determined by identifying the area of potential ground impact by means of a Monte Carlo approach, where the distribution of impact points is empirically determined by perturbing initial position and velocity according to a given navigation error distribution, assumed known.

Figure 4 represents a simple two-dimensional example. The nominal flight condition is horizontal flight at velocity V_0 and height h_0. Gaussian distributions for altitude error δh, velocity error δV and climb rate error $\delta \dot{h}$ are assumed, with standard deviation (STD) respectively equal to σ_h, σ_V, and $\sigma_{dh/dt}$. The resulting distribution of impact points around the nominal one is given by the bar chart, which is well approximated by

a Gaussian distribution (black solid line). In this way, the distribution of impact points x_I is described by means of the STD σ_x of the distance $\Delta x = x_I - x_N$ of impact points from the position of the nominal one, x_N.

An analogous approach is adopted for the three-dimensional scenario, where also lateral deviations from the prescribed flight path and lateral airspeed components are included among navigation errors. In this case, the empirical distribution of impact points on the ground, with coordinate (x, y) around the nominal one $(x_n, 0)$, obtained from a Monte Carlo simulation, can be approximated by a bi-variate Gaussian probability density function (PDF), $p(x, y)$, in the form:

$$p(x,y) = \frac{1}{2\pi\sigma_x\sigma_y\sqrt{1-\rho_{xy}^2}} \cdot \exp\left[-\frac{1}{2(1-\rho_{xy}^2)}\left(\frac{\Delta x^2}{\sigma_x^2} + \frac{\Delta y^2}{\sigma_y^2} - \frac{2\rho_{xy}\Delta x\Delta y}{\sigma_x\sigma_y}\right)\right]$$

where $\Delta x = x - \mu_x$, $\Delta y = y - \mu_y$, ρ_{xy} is the correlation between x and y, $\sigma_x > 0$ and $\sigma_y > 0$ are the STDs in the along-track and cross-track directions, respectively, and μ_x and μ_y their average values.

Figure 5 represents the results obtained from a Monte Carlo simulation to illustrate a three-dimensional case for a nominal flight condition in horizontal flight at velocity V_0 and height h_0 above the ground. In this case, Gaussian distributions are assumed for all the relevant navigation error variables, namely δh, δV and $\delta\dot{h}$ in the longitudinal plane (which contains the local vertical and the nominal velocity vector), with STD equal to σ_h, σ_V, and $\sigma_{dh/dt}$, whereas errors δy and δv in the cross track direction (perpendicular to the longitudinal plane) have a STD equal to σ_s and σ_v, respectively.

Note that, in the absence of realistic simulations or experimental data, all the navigation errors are assumed as independent uncorrelated statistical variables. This is another simplifying assumptions, as long as in the presence of deviations from the nominal flight path, velocity components are expected to be more likely oriented towards the nominal flight path, because of the action of the GNC system. A more accurate and realistic statistical distribution of navigation errors may be used, once available, without significant changes in the methodology proposed.

Discretization of the PDF When the distribution of impact points is determined by means of the statistical approach, it is necessary to consider that the probability of hitting a person inside the SIF is no longer uniform, as in the deterministic case (1 inside the DLA, 0 outside). The contour lines of the SIF are approximated by means of ellipses with semiaxes equal to $N\sigma_x$ and $N\sigma_y$ in the along- and cross-track directions, respectively. For $N = 3$, the SIF contains as many as 98.9% of the randomly distributed impact points. Two inner ellipses, with semiaxes equal to $\sigma_{(\cdot)}$ and $2\sigma_{(\cdot)}$, respectively, are also considered, such that the innermost ellipse contains 39.4% of the impact points, whereas the intermediate one 86.5%. Therefore, the probability of impact inside the 1σ ellipse is 39.4%, the probability of impact between the 1σ and the 2σ ellipses is 47.1% (that is, almost half of the sample lies inside the area between these ellipses), and the probability of impact between the 2σ and the 3σ ellipses is 12.4%. A fraction of approximately 1.1% of the sample lies outside of the 3σ ellipse, a portion that will be assumed negligible in the risk analysis and spread over the inner ellipses.

In order to define an efficient numerical procedure for risk assesment, the probability density is assumed constant inside each ellipse. This is equivalent to approximate the

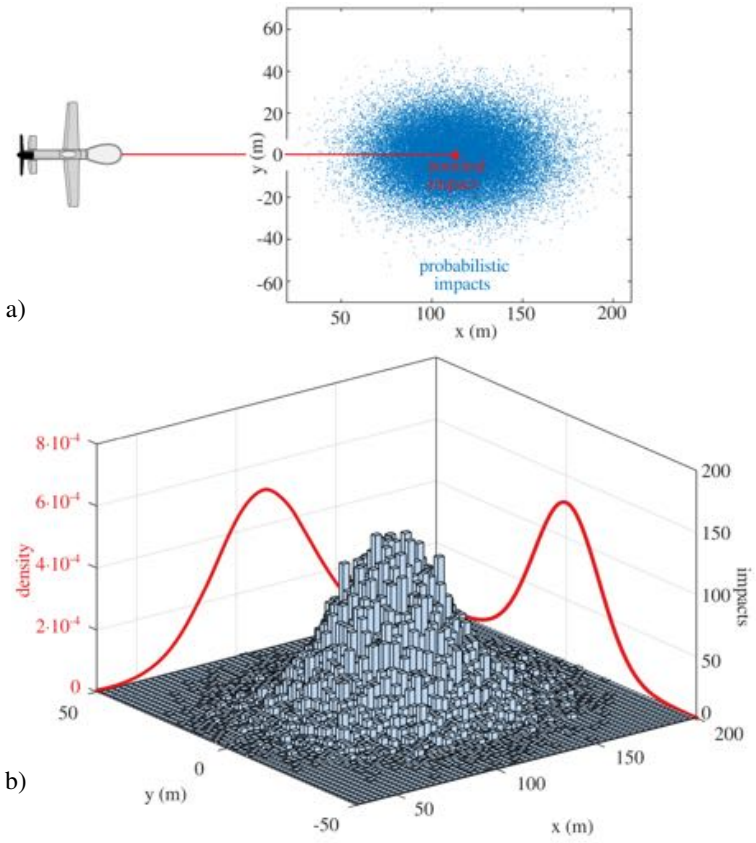

Figure 5. Statistic impact footprint for parabolic trajectories (illustrative 3-D example): distribution of impact points from a Monte Carlo simulation (a) and 3-D view of the resulting histogram, with projections of the approximated normal distribution (b).

probability density of impact points around the nominal one by means of a discrete version of the PDF, as depicted in Fig. 6, where the dispersion of impact points obtained from a Monte Carlo simulation (Fig. 6.a) is described by means of the three ellipses shown in Fig. 6.b, with σ, 2σ and 3σ as semiaxis. The discrete distribution is represented in Fig. 6.c. Once the probability of impact inside the area covered by each ellipse is known, the next step is to determine the time spent by a point on the ground inside each one of the ellipses, as a function of the characteristics of the trajectory element considered.

A Non-Dimensional Description of SIF The SIF for the three-dimensional case depends on the values assumed by a total of 8 variables, namely 3 initial values for velocity, altitude and climb rate (V_0, h_0 and $\dot{h}_0$), and 5 STDs for navigation errors (σ_h, σ_V, $\sigma_{dh/dt}$, σ_s, and σ_v). By applying the principles of dimensional analysis, it is possible to perform the statistical study of the SIF by means of nondimensional values

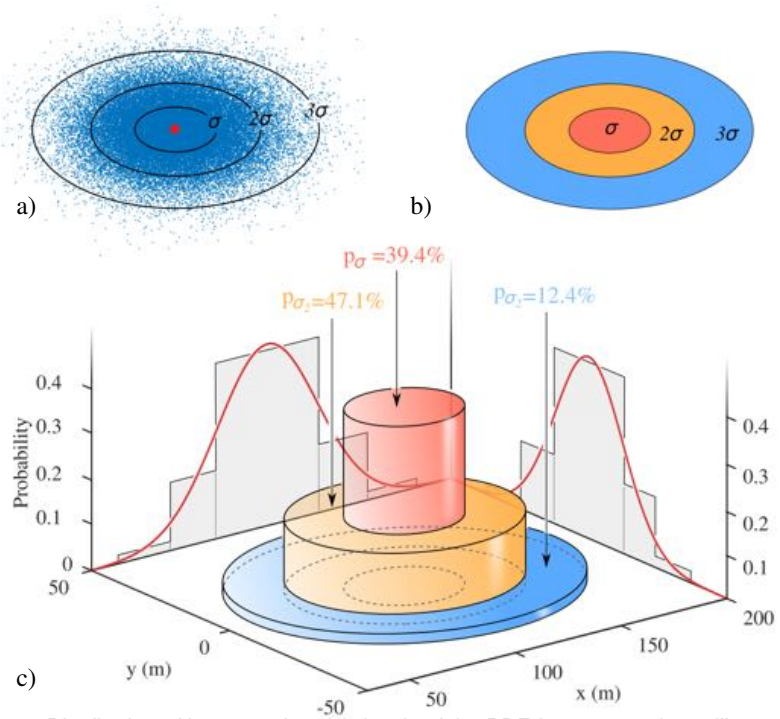

Figure 6. Distribution of impact points (a), levels of the PDF for σ, 2σ and 3σ ellipses (b) and probability levels for a single normally distribute random variable (c).

for all the relevant variables, simply scaling STDs for displacement errors with respect to h_0 and STDs for velocity variables with respect to V_0, that is

$$\hat{\sigma}_s = \sigma_s/h_0\,;\;\; \hat{\sigma}_h = \sigma_h/h_0\,;\;\; \hat{\sigma}_V = \sigma_V/V_0\,;\;\; \hat{\sigma}_{dh/dt} = \sigma_{dh/dt}/V_0\,;\;\; \hat{\sigma}_v = \sigma_v/V_0$$

As far as initial conditions are concerned, a nondimensional energy ratio parameter and a nondimensional altitude parameter are introduced, namely

$$\Pi = V_0^2/(gh_0)\,;\;\; \hat{h} = h_0/h_P$$

The former is equal to twice the ratio between initial vehicle kinetic energy and its potential energy, evaluated with respect to ground level. The latter scales the initial altitude with respect to the altitude assumed for the average person in the area. Monte Carlo simulations where performed using the non-dimensional parameters, so that all variables were scaled and the number of plots and relevant variables reduced. The results are described in the next subsection.

Analysis of the Risk Assessment Approaches

Comparison of the Expected Impact Areas The solid lines in Figs. 7 and 8 represent the length $L = 3\sigma_x$ and the width $W = 3\sigma_y$ of the SIF, respectively, determined

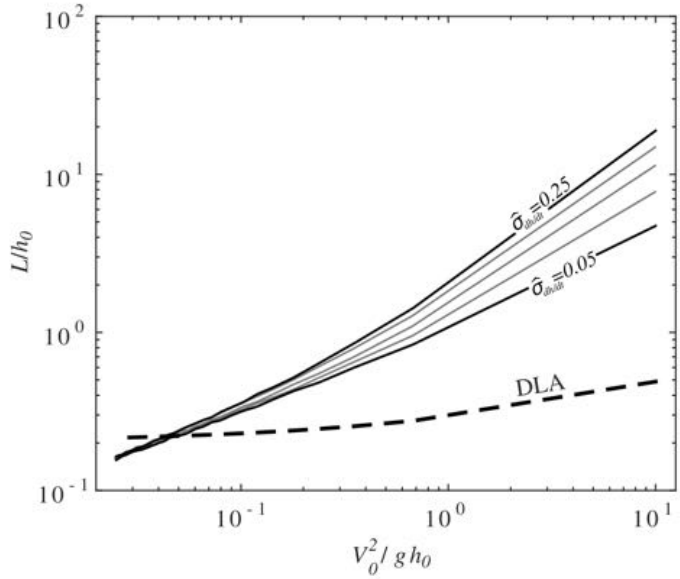

Figure 7. Length of the 3-σ_x SIF for $\hat{h} = 30$ and different values of $\hat{\sigma}_{dh/dt}$, compared with the length of the DLA (dashed thick line).

for ballistic trajectories, for different values of the energy parameter Π and non-dimensional values of the standard deviation of navigation errors. Obviously, the size of the ellipse enclosing the SIF increases for higher values of navigation errors (which means a wider dispersion of the initial conditions at failure) and higher values of the energy parameter (which means higher values of velocity for a given altitude). In the same figures, the black thick dashed lines in represent the length (Fig. 7) and the width (Fig. 8) of the DLA. As discussed previously, the latter depends on the size of the vehicle, and it is thus independent of the initial condition, whereas the former slightly increases with Π, as a result of the combination of a steeper descent angle for higher altitudes and a smaller glide slope for higher velocities.

All the reported cases clearly show that, for the selected values of standard deviation of the non-dimensional navigation error variables, the size of the DLA is significantly smaller than that of the SIF, unless very small values of Π are dealt with, which are realistic only for very small values of airspeed, that is, for rotorcraft at or close to a hovering condition. This first result already shows that the use of the DLA may underestimate the risk, if a more densely populated area is close to the area of operations and that area lies outside of the DLA, but it can be reached because of navigation errors at the beginning of the uncontrolled fall.

Limitation of the two approaches The analysis presented in this paper is based on a few simplifying assumptions, that are now critically reviewed. First of all, the trajectory after failure is assumed parabolic, as if only gravity acts on the vehicle. This implies that no aerodynamic force dissipates energy during the fall, nor gliding flight

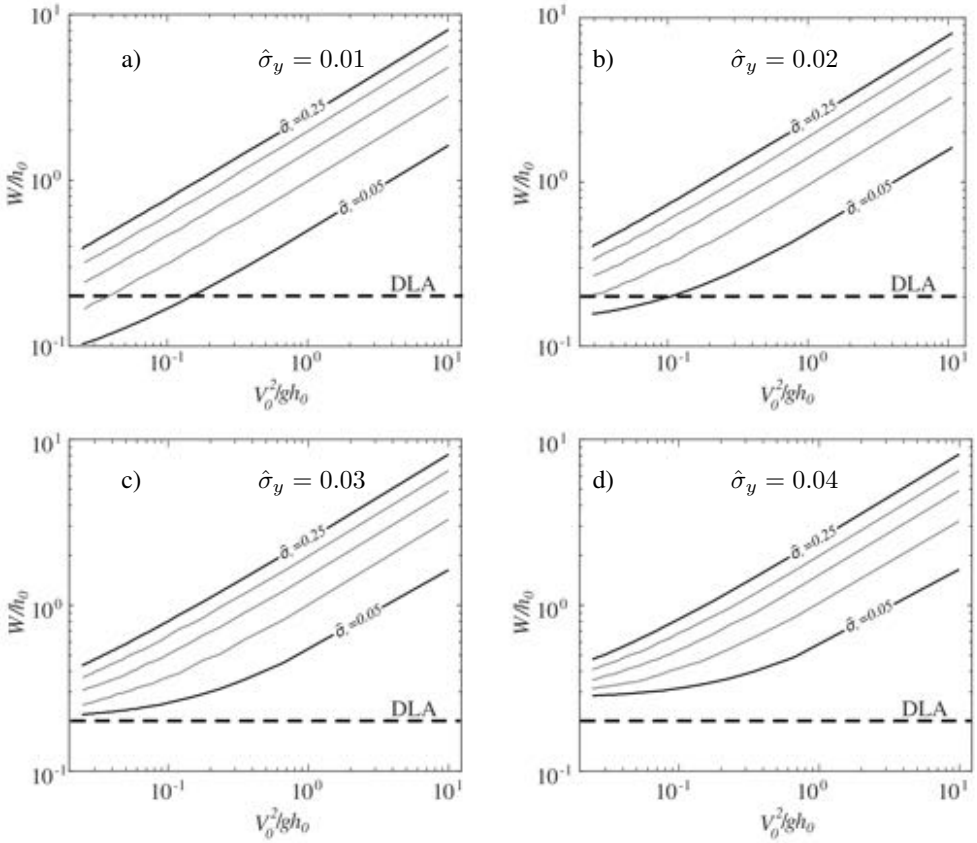

Figure 8. Width of the 3-σ_y SIF for $\hat{h} = 30$ and different values of $\hat{\sigma}_y$ and $\hat{\sigma}_v$, compared with the width of the DLA (dashed thick line)..

is considered. In the presence of a gliding steady state the distance covered after failure may become considerably longer, and more seriously affected by wind and turbulence. Hence, the dispersion of the impact points is expected to become significantly wider, and dependent on unpredictable environmental conditions.

In the presence of wind and turbulence, the definition of the SIF for gliding trajectories would require to be thoroughly reconsidered by an *ad hoc* set of Monte Carlo simulations, where wind gradients and turbulence of various intensities are included in a 6 degree-of-freedom model of the vehicle. This analysis would be computationally demanding, but it can be performed only once, in order to identify the relation between the parameters used for environmental disturbance and their effect on the dispersion of the impact points. If the resulting bar chart of impact points still follows (at least approximately) a Gaussian bivariate distribution, once the standard deviations for the dispersion points in the along-track and cross-track directions are known, all the remaining parts of the analysis remain virtually unchanged. Similarly,

the effects of wind and turbulence on navigation errors can be included into the dispersion data used for the determination of the random initial condition. In such a case, a further Monte Carlo analysis would be required and/or data taken from actual UAS telemetry records, which highlight the effect of environmental condition on trajectory tracking precision.

Also, no fragmentation prior to impact is considered, which means that the vehicle is assumed to fall to the ground in one piece. This rules out the possibility of analyzing the risk of a catastrophic failure due to an explosion, as well as the effect of a flight termination system based on a self-destruction procedure. Nonetheless, such a scenario rules out most of the issues related to the presence of wind and gliding trajectories after failure, provided that most of the fragments will be expected to follow a quasi-parabolic trajectory. The statistical impact footprint becomes obviously more complex, where more statistical data need to be included in the Monte Carlo analysis, such as the number of fragments, their size, and their initial conditions after the explosion. Nonetheless, a statistical impact footprint of debris could still be introduced, once the distributions of number of debris per unit area and kilograms (or Joule) of debris per unit area is determined in simulation or by experiments.

As a final observation, when the presence of uncertainties such as the effects of wind and turbulence or fragmentation become a relevant factor for the risk assessment procedure, the approach based on the DLA becomes less interesting, provided that none of these effects can be included in any way in the analysis.

Risk evaluation for motion primitives

Risk Evaluation by means of the DLA The risk of hitting a person standing at point P on the ground is proportional to the time spent by point P inside the DLA when the UAS flies in the neighbourhood, assuming that, as stated before, the probability of being hit after a catastrophic failure in the deterministic case is equal to 1, if one stands inside the DLA. The evaluation of risk is thus performed by means of a 2 step procedure:

1. identify the boundaries of the DLA corridor, that is the portion A of the ground surface made of points P that spend a time $t_e > 0$ inside the DLA;
2. evaluate the exposed time t_e, that is, how much time is spent by each area element $\mathrm{d}A$ of A inside the DLA.

Step 1 provides the boundaries of the risk corridor, that is the area swept by the DLA. For that purpose, the boundaries of the corridor (see Figs. 9.a and 10.a) are discretized as a series of spaced points. A cell of the population density grid is considered to be crossed or touched by the risk corridor if at least one of the sampled points along the boundaries lies inside it. The distance between discrete points along the corridor boundary is kept constant and equal to 5 m. Such a value guarantees that, in the worst case – when only one boundary of the corridor crosses a grid cell without any point being inside the cell – the maximum risk area that could be discarded in the process is a corner of approximately 6 m^2 (0.06% of the total cell area).

Step 2 allows for the evaluation of the total risk, once the trajectory flown by the UAS is known. In what follows, two cases will be considered: rectilinear elements and

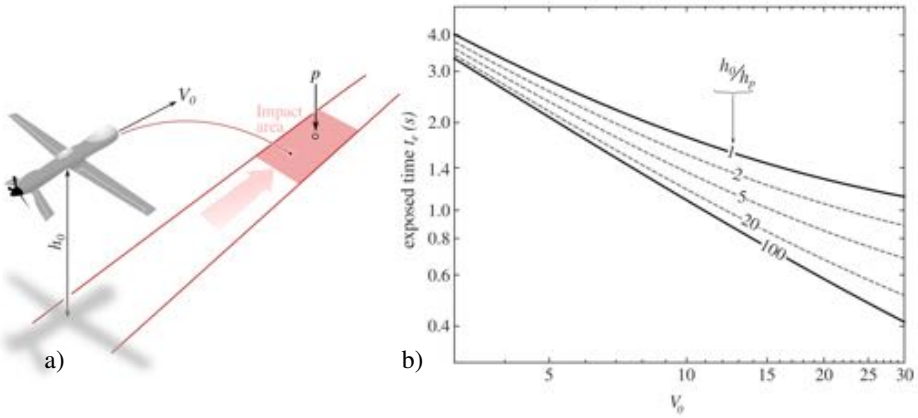

Figure 9. Time spent by a point P on the ground inside the DLA for a rectilinear primitive: sketch (a) and plot of t_e vs V_0 for various $\hat{h}$.

curved ones. As a matter of fact, the position of the DLA with respect to the nominal trajectory flown by the vehicle depends on altitude and initial velocity only, but its motion on the ground follows the trajectory. When a curved trajectory is considered, the position of the DLA on the ground is no longer symmetric with respect to the projection of the trajectory on the ground. Hence the exposed time t_e of points on the curvature radius at various distances from the ground track varies.

For the sake of simplicity the evaluation of t_e is performed approximating the DLA by means of a rectangle which envelopes the DLA. The resulting size of the rectangle is thus a length $\ell = \sqrt{7}\,(2r_p + L + h_P/\tan\gamma)$ and a width $d = \sqrt{7}\,(2r_p + L)$. Hence, the area of the DLA is $A_\ell = \ell \cdot d$.

Rectilinear segments For a rectilinear motion primitive the DLA sweeps a corridor of width d, equal to that of the DLA itself, placed symmetrically with respect to the ground projection of the trajectory (Fig. 9.a). Assuming the rectangular approximation of the DLA, the time spend by the DLA over each point inside the corridor swept is independent of the distance from the ground projection of the trajectory, and it is equal to $t_e = \ell/V$. For a ballistic trajectory, it is possible to evaluate t_e as a function of initial speed V_0 and altitude (reported in terms of nondimensional altitude parameter $\hat{h}$). The plots reported in Fig. 9.b are obtained, which all diverge towards infinity, as $V_0 \to 0$ (hovering condition), with a monotonously decreasing value as V_0 increases. In the logarithmic scale adopted for V, the variation of t_e with V_0 is a straight line for very high initial altitudes.

When the actual shape of the DLA is adopted, t_e is slightly reduced at the bounds of the corridor, where the DLA is shorter than ℓ, with respect to the value achieved at the centerline, where the DLA is maximum and equal to ell. These variations are minor for most realistic values of V_0 and γ_0 and their relevance in the overall risk assessment process does not justify the additional mathematical complexity. Moreover, the risk is (slightly) overestimated with the simplified DLA rectangular shape, hence the overall risk evaluation is conservative.

a)

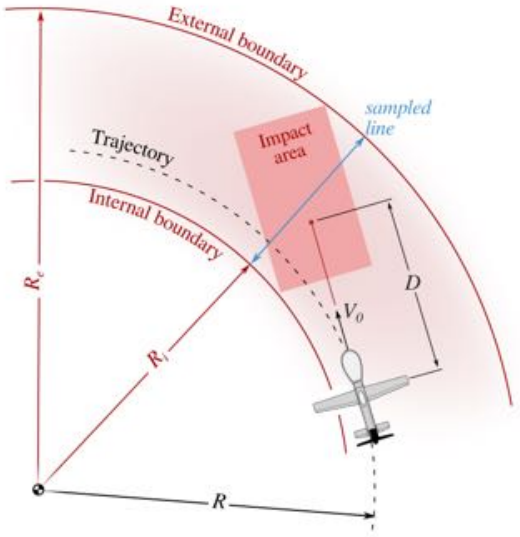

b)

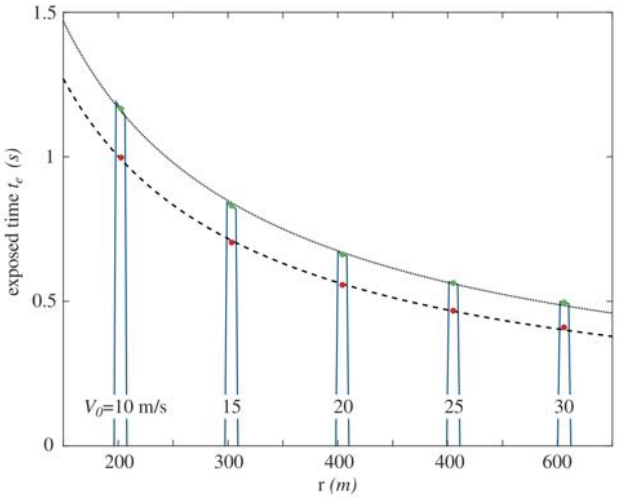

Figure 10. Time spent by a point P on the ground inside the DLA during a turn: sketch (a) and plot of t_e vs r for $\dot{\chi} = 0.1$ rad/s and $h_0 = 40$ m.

Turning maneuvers When a turning motion primitive is dealt with, the parabolic fall drives the vehicle away from the pattern of the ground projection of the trajectory (Fig. 10.a). The use of the rectangular approximations, in this case, greatly simplifies the determination of the boundaries of the risk corridor, where, independently of the radius of curvature $R = V/\dot{\chi}$ of the trajectory, the outer boundary is represented by the trajectory of one of the top corners of the DLA, whereas the inner one is obtained from the trajectory of one of its bottom corners. By means of elementary

geometrical considerations, it is possible to determine the radii of curvature of the internal and external boundaries of the corridor, indicated as R_i and R_e, respectively. Letting D be the distance covered during the parabolic fall, $L_s = \sqrt{7}\,(r_p + b/2)$, $L_b = d\left(\sqrt{7} - 1\right) + L_s$ and $L_r = d + L_s$, one has that

$$R_i = \sqrt{(R - L_s)^2 + (D - L_r)^2}\,; \;\; R_e = \sqrt{(R + L_s)^2 + (D + L_b)^2} \qquad (8)$$

The exposed time t_e is greater than 0 for points lying at a distance r from the center of curvature such that $R_i \leq r \leq R_e$. The variation of t_e vs. r for $\dot{\chi} = 0.1$ rad/s, $h_0 = 40$ m and 5 different values of V_0 is reported in Fig. 10.b. Unless the radius of curvature becomes very small, in the same order of magnitude of the width of the DLA, the variation of t_e with r is very steep at the bounds of the risk corridor and almost constant at the center of it. In order to simplify risk evaluation, a uniform value of t_e, equal to its average value, can be assumed in the interval $R_i \leq r \leq R_e$. If one wishes a more conservative estimate of the risk, it is possible to assume that t_e is equal to the average value of the peak segment.

In both cases it is possible to observe that the variation of t_e with $r = V/\dot{\chi}$ is well captured by an exponential curve fit in the form $t_e = Ar^{\alpha}$, where the coefficients A and α are evaluated by means of a least square approximation. For the case considered, the coefficients are equal to $A = 79.4$ and $\alpha = -0.83$, when the average value of t_e is considered (dashed thick line in Fig. 10.b), and $A = 78.1$ and $\alpha = -0.79$, when t_e is assumed equal to the average of the peak segment (dotted line in Fig. 10.b). These values depend on h_0/h_P and $\dot{\chi}$, and the approximation can be used within the bounds R_i and R_e of the risk corridor, which can be evaluated from Eq. (8).

The resulting values of the average t_e vs. V_0 for several values of the initial altitude, h_0, and different values of the turn rate $\dot{\chi}$ are reported in Figure 11. Similar values are obtained if the average peak value is adopted in the approximation. The behaviour of the curve when the angular speed is smaller (hence R larger), reported in Fig. 11.a closely resembles that reported in Fig. 9.b for a rectilinear segment. The shaded areas in Figs. 11.c and d represent values of velocity which determine a radius of curvature in the same order to magnitude of DLA width. In this case t_e rapidly diverges towards infinity and the uniform approximation of t_e is no longer valid. Such a situation occurs only for rotorcraft flying at slow speed, in which case the exposed time becomes equal to the time spent by the vehicle above the considered point at zero or quasi-zero velocity, or for (possibly unfeasible) very high angular rates, as in Fig. 11.d.

Risk Evaluation by means of the DLA The risk corridor is represented by the strip of ground swept by the deterministic lethal area during the nominal motion of the UAS. The first step of the risk evaluation procedure is thus the identification of all the grid elements crossed by the risk corridor. The intersection of the risk corridor with the population density grid divides the corridor into a set of elements, which will be numbered. from 1 to M. The generic element will be associated to the index i.

For rectilinear segments the shape can be rectangular, trapezoidal, rhomboidal or triangular. More complex shapes can occasionally be found when the nominal flight path intersects the grid close to one or two corners of the grid element. In all cases it is possible to determine analytically the intersection points of the boundaries of the corridor with the grid and the area of each element becomes thus known. For turning

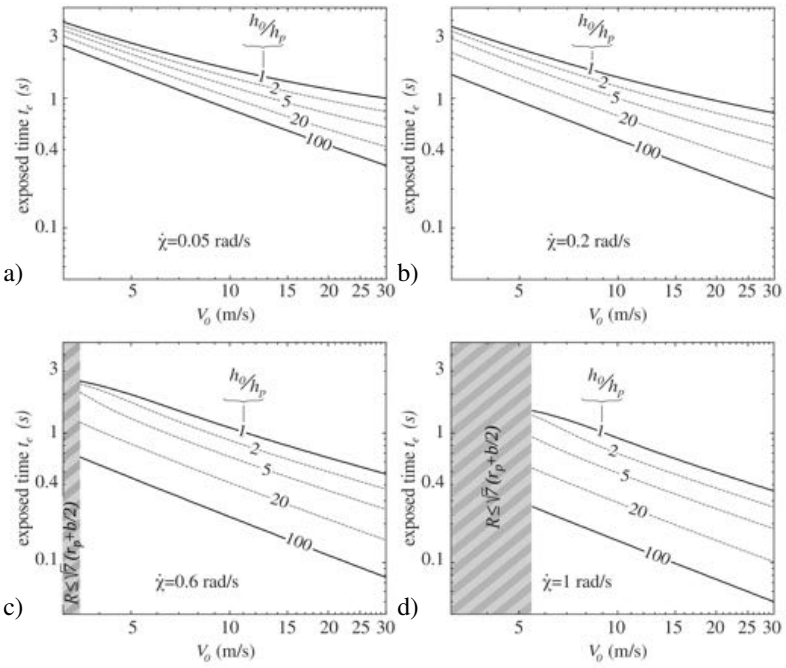

Figure 11. Ground exposed time during turning maneuver as a function of V_0 and h_0/h_P for $\dot{\chi}$=0.05, 0.2, 0.6 and 1 rad/s.

maneuvers, the shape of the resulting elements is more complex, with arcs as well as segments as elements of the boundary. In this case the area is evaluated numerically, approximating the curved elements of the corridor boundaries with a polygon sampled with the same spatial frequency adopted for the trajectory.

Following the simplifications and assumptions discussed in the previous paragraphs, t_e is assumed constant over the entire width of the risk corridor and the whole length of the segment (along which velocity is constant), for both straight and curved corridor elements. The probability of falling inside one of the elements is thus proportional to the product of t_e times the area of the element. The total risk of hitting somebody after a catastrophic failure is evaluated by summing up all the contributions obtained from the area elements of the entire risk corridor, from the beginning to the end of the mission.

The risk value associated to the j–th motion primitive is determined by the sum of the risk values inside each one of the grid cells i exposed to the DLA along the path of the j–th primitive, that is:

$$\Gamma_j = p_F \sum_i A_\ell (t_i/t_M)\rho_i$$

where t_M is the total mission time, t_i is the time that the DLA remains inside the i–th grid cell, A_ℓ is the size of the lethal area and ρ_i the population density in the cell. If one considers rectangular elements for the risk corridor, with length $L_{c,i}$ and width d,

the exposed time t_e defined above for the rectangular approximation of the DLA, such that $A_\ell = d \cdot \ell$, each term in the above sum can be rewritten as follows:

$$A_\ell \frac{t_i}{t_M} \rho_i = (d \cdot \ell) \frac{L_{c,i}/V}{t_M} \rho_i = (d \cdot L_{c,i}) \frac{\ell}{V} \frac{1}{t_M} \rho_i = A_{c,i} \frac{t_e}{t_M} \rho_i$$

where $A_{c,i}$ is the area of the risk corridor element inside of the i–th cell. Note that the last form can be extended to non rectangular shapes of the corridor element inside cell i, whereas the first is not generalizable. Hence the last one will be adopted for the evaluation of risk for a generic trajectory in the next paragraph.

Risk Evaluation by means of the SIF

General aspects When the risk is evaluated on the basis of a statistical impact footprint, discretized by means of 3 ellipses, as described in the previous paragraph, the evaluation of the risk follows a slightly different pattern. First of all the three ellipses with semimajor axes $k\sigma_x$ and $k\sigma_y$ ($k = 1, 2, 3$) determine 3 risk corridors. For each one of the corridors, the procedure presented in the previous subparagraph is repeated, in order to identify the cells of the population density grid crossed by each one of the corridors. This part of the procedure is identical to that defined above for the DLA (although repeated three times, for increasingly wider corridors) and it is not repeated here. In the following paragraphs, the details on the evaluation of the exposed time to an elliptical area along rectilinear and turning motion primitives and the resulting procedure for the determination of the overall risk along the trajectory will be discussed.

Rectilinear segments For a motion primitive, the ellipses sweep a corridor with a width equal to the axes of the ellipses in the cross-track direction, namely $d_k = k\sigma_y$, with $k = 1, 2, 3$. The distribution of exposed times in the cross-track direction between the boundaries of the corridor for the k–th ellipse is equal to

$$t_{e,k}(y) = L_k(y)/V_0$$

where $L_k(y)$ is the length of the k–th ellipse in the along-track direction at a coordinate y, with $L_{k,\max} = 2k\sigma_x$. An illustrative example is reported in Fig. 12.a. The distribution of exposed time $t_{e,k}$ as a function of the cross-track distance y from the nominal impact point is represented by a semi-ellipse, as shown in Fig. 12.b. The exposed time distributions depicted in Fig. 12.b thus provide the time that a point on the ground spends inside each ellipse as a function of its distance in the core-track direction from the trajectory of the nominal impact point (which, for a rectilinear segment, coincide with the ground track of the vehicle trajectory).

The probability that a point on the ground is hit by the failed vehicle is proportional to the time spent inside one ellipse, weighted by the overall probability level associated to that ellipse. For the discretization of the Gaussian bivariate distribution described in the previous section, the total probability becomes proportional to the equivalent exposed time, defined as

$$t_{e,e} = t_{e,1} p_\sigma + (t_{e,2} - t_{e,1}) p_{2\sigma} + (t_{e,3} - t_{e,2}) p_{3\sigma}$$

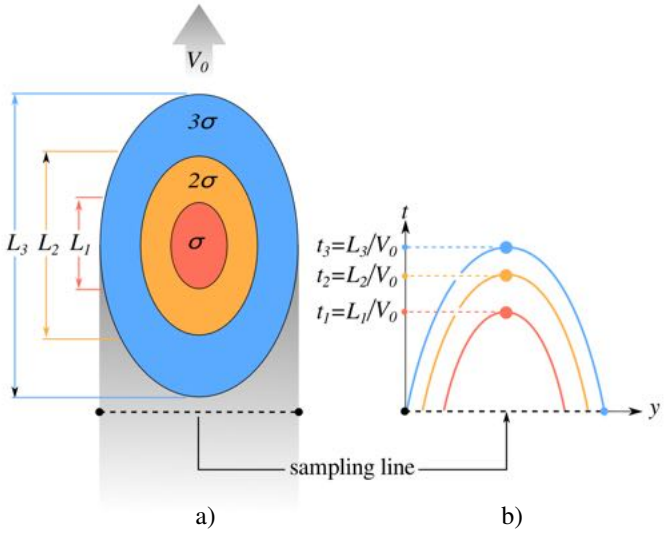

Figure 12. Time distribution of the exposed time in a rectilinear segment: ellipses dimensions (left) and time values for each ellipse (right).

represents a weighted combination of the time $t_{e,k} - t_{e,(k-1)}$ spent inside the k–th ellipse, but outside the $(k-1)$-th one. The weights $p_{k\sigma}$, $k = 1, 2, 3$ are equal to the expected fraction of crash points inside the k–th ellipse and outside the $(k-1)$–th one. For the present discretization of the Gaussian bivariate distribution one has that $p_\sigma = 0.394$, $p_{2\sigma} = 0.471$, and $p_{3\sigma} = 0.124$, assuming uncorrelated random variables.

As an example, consider a ground point placed at the center of the ellipse trajectory. Such a ground point will be exposed to the σ ellipse for a time equal to L_1/V_0, which is the time that the point remains inside the ellipse. The time spent inside the ellipse 2σ is equal to the time that the point remains inside the ellipse 2σ minus the time that the point is inside the σ ellipse , that is, $(L_2 - L_1)/V_0$. Similarly, the point is exposed to the 3σ ellipse for a time equal to $(L_3 - L_2)/V_0$. The distance of the ground point from the ground-track determines if it is overpassed by three, two, only one or none of the ellipses.

Turning maneuvers In the case of a turning maneuver, the determination of the exposed time of a ground point to each one of the ellipses is less trivial. An illustrative sketch of the problem for a single ellipse is shown in Fig.13.a. The ellipse turns around the flight path center of rotation C with radius R. The movement of the k–th ellipse creates a corridor defined by an internal and an external boundary, with radius equal to $R_{i,k}$ and $R_{e,k}$, respectively. The radius of the corridor centerline, that is, the path of the ellipse center, is then $R_c = {}^1/_2(R_{i,k} + R_{e,k})$. The exposed time is greater than zero for those points such that the distance r from the center of rotation C is $R_{i,k} < r < R_{e,k}$, becoming zero at the bounds. The exposed time is equal to

$$t_e = \alpha(r)/\dot{\chi}$$

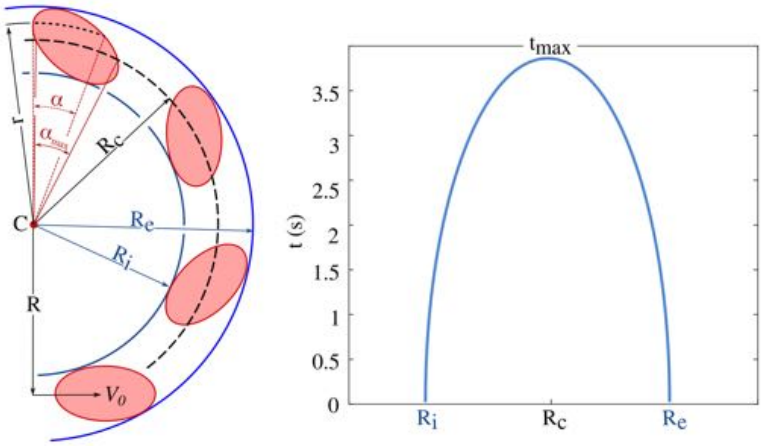

a) b)

Figure 13. Time distribution of the exposed time in a turning maneuvers: parameters definition (a) and t_e vs r plot (b).

where $\alpha(r)$ is the amplitude of the arc centered in C and enclosed in the ellipse at a distance r from C (Fig. 13.a). The value of t_e is maximum for $r = R_c$.

The values of the bounds $R_{i,k}$ and $R_{e,k}$ of the corridor and $t_{\max}$ are evaluated by discretizing the ellipse by means of a finite number of points. The distance of the point closest to C provides an estimate of $R_{i,k}$, whereas distance of the farthest point is the estimate of $R_{e,k}$. The points such that the distance from C is closest to R_c provide the directions of the bounds of the widest arc, $\alpha_{\max}$, from which $t_{\max}$ is estimated. The resulting exposed time distribution along a radial line, reported in Fig.13.b, is again provided by half of an ellipse,

$$t_e(r) = t_{\max}\sqrt{1 - [(r - R_c)/(R_e - R_c)]^2}$$

The accuracy in the evaluation of $t_{\max}$, $R_{i,k}$ and $R_{e,k}$ depends on the number of points used to discretize the ellipse. In the present work the ellipses are discretized by means of 100 points. Results change by less than 0.05% by increasing the number of points from 100 to 1000. The computational effort of this phase is negligible compared with that necessary for the Monte Carlo simulation. The procedure needs to be performed for all of the three ellipses. Once the exposed time t_1, t_2 and t_3 as a function of r, for $R_{i,k} < r < R_{e,k}$ are available, a weighted combination as in the previous, rectilinear, case allows for the definition of a total equivalent exposed time at each radial distance r within the corridor.

Risk Evaluation Three different risk corridors are defined, one for each of the 3σ, 2σ and σ ellipses, along the nominal trajectory of the UAS. An algorithm identical to the one used for the DLA corridor described above allows for the identification of the intersections between the areas of the corridor and the grid cells. Figure 14 shows an illustrative sketch of the three corridors and the corresponding areas, each one with a different color, in a cell grid.

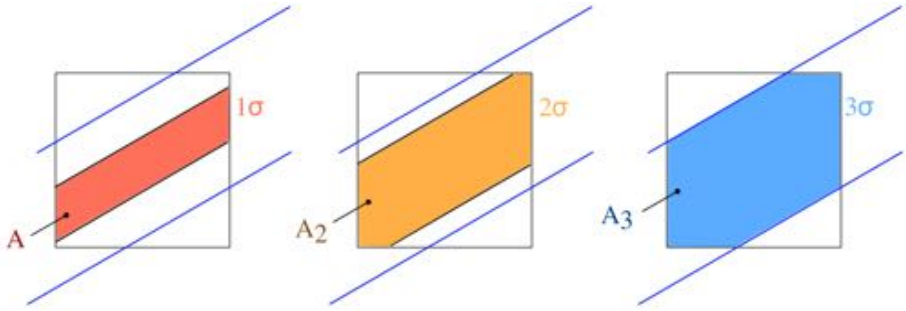

Figure 14. The three corridors inside a grid cell

For each cell, the net area of each corridor, – that is, the area of the corridor, excluding the area of the smaller corridor(s) inside, when present – must be multiplied by the associated impact probability and the equivalent exposed time (see above for the definition of $t_{e,e}$). But when the statistical impact footprint is used for the determination of the potential impact points in the presence of navigation errors, an accurate procedure for the evaluation of $t_{e,e}$ is complex and computationally demanding. If on one side a discretization procedure of each area element could be used once the mission profile is chosen, the computational cost makes it ill-suited (and possibly inapplicable) in the framework of an optimization tool. Nonetheless, it is still possible to obtain a reasonable estimate, assuming an average value of the exposed time $t_{e,k}$ inside each one of the three corridors. The approach based on the average exposed time provides a computationally efficient algorithm, which exploits a technique similar to that outlined above for the DLA.

The equivalent averaged exposed times of a point inside each one of the corridors are given by

$$\begin{aligned} t_{e,c_1} &= t_{1,c_1} p_\sigma + (t_{2,c_1} - t_{1,c_1}) p_{2\sigma} + (t_{3,c_1} - t_{2,c_1}) p_{3\sigma} \\ t_{e,c_2} &= (t_{2,c_2} - t_{1,c_2}) p_{2\sigma} + (t_{3,c_2} - t_{2,c_2}) p_{3\sigma} \\ t_{e,c_3} &= t_{3,c_3} p_{3\sigma} \end{aligned}$$

where t_{k,c_m} corresponds to the average exposed time to the ellipse $k\sigma$ of a point standing inside the corridor $m\sigma$.

The risk value associated to the j–th flight primitive is determined as the sum of the risk values in each one of the grid cells i exposed to the SIF, that is

$$\Gamma_j = p_F \sum_i A_\ell \left(\frac{A_{1,i}}{A_\sigma} t_{e,c_1} + \frac{A_{2,i}}{A_{2\sigma}} t_{e,c_2} + \frac{A_{3,i}}{A_{3\sigma}} t_{e,c_3} \right) \frac{1}{t_M} \rho_i$$

where A_σ, $A_{2\sigma}$ and $A_{3\sigma}$ are respectively the areas of the σ, 2σ and 3σ ellipses, $A_{1,i}$, $A_{2,i}$ and $A_{3,i}$ are the areas of each risk corridor in the corresponding grid cell i.

Equivalence of approaches over uniform areas In spite of the different risk assessment approaches, both of them provide the same results when the population

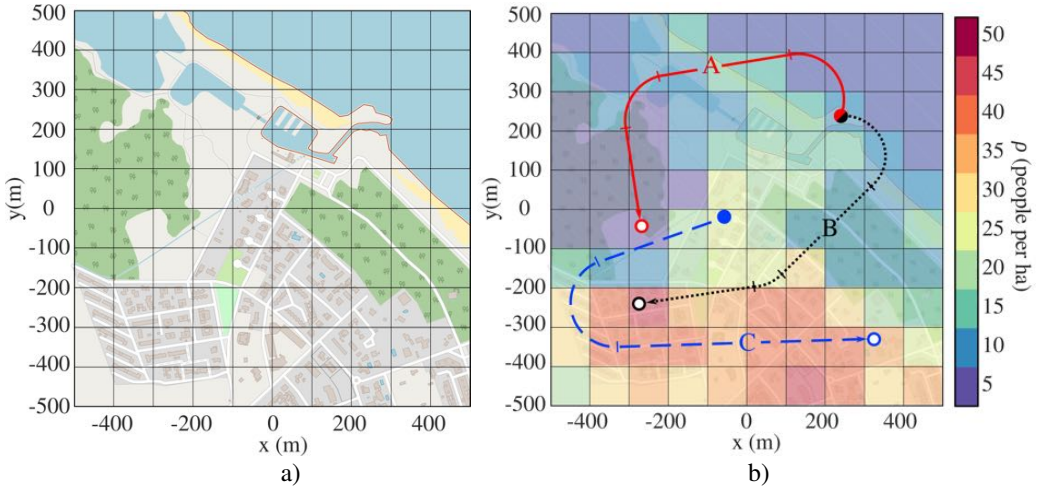

Figure 15. Area of the sample mission scenario (a) with population density grid and tested trajectories A, B and C (b).

density is uniform. The difference between the DLA and the SIF approaches is that in the latter case position and velocity of the UAV are described by means of a probabilistic density functions, which leads to a probabilistic distribution of the impact points. But when the vehicle hits the ground, the risk will once again be concentrated inside the lethal area. The SIF approach simply distributes the potential locations where the UAV may impact from a deterministically known point to an area, inside which different risk probabilities are present, but the total risk is the same. If the population density is uniform, it simply does not matter where the UAV will actually fall as the risk of hitting someone would be the same everywhere, the product of $A_c \cdot \rho_i$ being the same. The situation is different when ρ is not uniform inside the operational area. In such a case the probabilistic impact area of the SIF may include cells not considered in the DLA corridor where density (hence risk) is either higher or lower, thus increasing or mitigating the risk. If these cells have a significantly higher population density then the total risk value may vary significantly with respect to the value determined by the DLA approach.

Results

Test cases and trajectories

As an example, the methodology is applied to a fictitious mission scenario taking place in the area depicted in Fig. 15(a). The area is a square with a side equal to 1 km. A 10×10 square grid, with cells 100×100 m (that is, 1 hectare of surface) is used for providing information on population density, assumed known and uniform inside each grid cell, ranging from a maximum greater than 50 persons per hectare down to a minimum below 5 persons per hectare, as depicted in Fig.15(b).

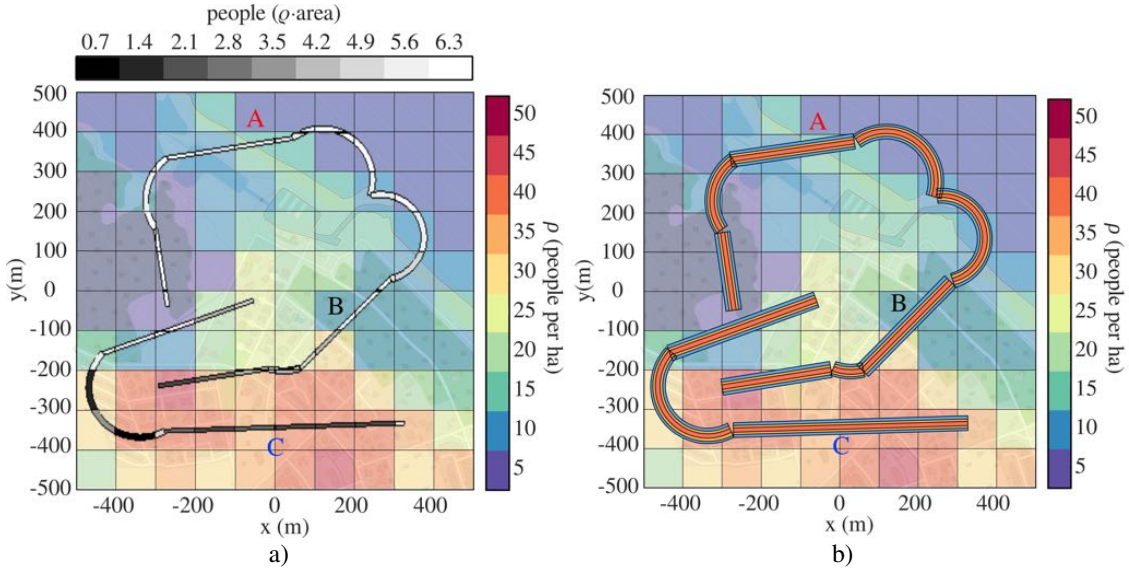

Figure 16. Elements of the risk corridor for the DLA approach (a) and the SIF approach (b).

Three different trajectories were tested (Fig. 15(b)). The trajectory A overflies a lowly populated area. Trajectory B flies through a population gradient from a lowly populated area to an intermediate populated area. Finally, trajectory C flies over a densely populated area. For the sake of simplicity all the trajectories keep a constant velocity of 20 m s^{-1} and a constant height of 50 m. For each one of the trajectories the risk is evaluated by the DLA and SIF approaches.

Application of the DLA

The graphical result of evaluating the risk with the DLA approach to the scenario of Fig. 15 can be observed in Fig. 16(a), where the risk corridors are depicted. Inside each cell, the gray scale of the corridor corresponds to the product $\rho_i \cdot A_\ell$, where A_ℓ is the area of the corridor element inside the i–th cell. Since the velocity is constant for all the trajectories, also the exposed time t_e is constant, and the risk value can be considered simply proportional to $\rho_i \cdot A_\ell$. From Fig. 16(a), it is possible to observe that higher risk values are obtained when a large area is covered inside a highly populated cell.

Application of the SIF

Figure 16(b) shows the three risk corridors represented in Fig. 16 applied to the three trajectories A, B and C. Comparing the corridors width between Figs. 16(a) and 16(b), it is evident that the SIF significantly extends the limits of the potential area under risk. However, it must be remembered that the probability of impact is not equal across the corridor. In other words, the SIF highlights that in presence of navigation errors a larger

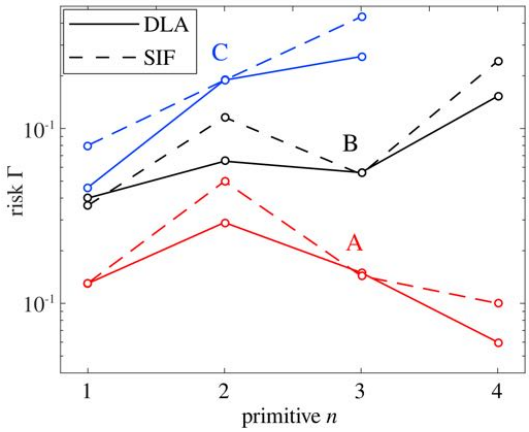

Figure 17. Comparison of risk values for the three trajectories tested showed in Fig. 14

ground area is exposed to an impact, but the impact probability is not evenly distributed inside the area at risk.

A numerical comparison of the results

A quantitative comparison between the DLA and the SIF approaches is performed, as reported in Fig. 17, where the risk values for each primitive element of the three trajectories tested obtained by means of both approaches is shown (solid lines for DLA, dashed ones for SIF). The overall risk trend of each trajectory appears independent of the approach, being affected only by the area covered by the trajectory. In other words, no major differences in the risk values are evident and a path results riskier than another independently of the approach adopted in the evaluation of risk.

Conclusions

A procedure for evaluating the risk of hitting a person while operating an Unmanned Aerial Vehicle over a populated area is proposed, assuming that the vehicle falls along a parabolic trajectory after a catastrophic failure. Two alternative approaches are developed for determining the area where the impact on the ground takes place: a deterministic approach, where the lethal area is determined as a function of vehicle size, kinetic energy and glide slope at impact; and a statistical approach, which takes into account the dispersion of impact points on the ground due to navigation errors, that is, discrepancies between the planned trajectory and that actually flown by the vehicle. In the first case, the risk at each point of the ground is simply proportional to the amount of time spent inside the lethal area, data that can be determined easily, once the kinematics of the vehicle along the planned trajectory is known. On the converse, the statistical approach requires a set of Monte Carlo simulations for the definition of the statistical impact footprint, an ellipse with semiaxes equal to three standard deviations of the distance of impact points in the along- and cross-track directions. The risk of being hit

is proportional to the amount of time spent inside the impact footprint multiplied by the probability level, discretized by means of the σ, 2σ and 3σ ellipses.

The two approaches are tested for an example test case, where the nominal trajectory is divided into motion primitives, that is, arcs or segments flown at steady state. The approaches proposed allow one to evaluate the total risk in a computationally efficient way, once system and trajectory parameters (and possibly statistical properties of navigation errors) are known. Results revealed the risk values determined by means of the statistical and the deterministic approach lie in the same order of magnitude. Both approaches lend themselves to the possibility of optimizing the trajectory, in order to minimize the total risk, mitigating it in those parts of the trajectory where it is higher and/or reduce it below a prescribed threshold.

Acknowledgments

This research was supported by the European Union and the Apulian Local Government through call FSC Cluster 2014, project Test and Knowledge-based Environment for Operations, Flight and Facility (TAKEOFF).

References

1. Weibel R and Hansman RJ. Safety Considerations for Operation of Different Classes of UAVs in the NAS. *AIAA 3Rd "Unmanned Unlimited" Technical Conference, Workshop and Exhibit* 2004; (September): 1–11.
2. Dalamagkidis K, Valavanis KP and Piegl LA. Evaluating the risk of unmanned aircraft ground impacts. *2008 Mediterranean Conference on Control and Automation - Conference Proceedings, MED'08* 2008; : 709–716.
3. Guglieri G and Ristorto G. Safety Assessment for Light Remotely Piloted Aircraft Systems. *2016 INAIR - International Conference on Air Transport* 2016; : 1–7.
4. Chen AZJ and Mo JPT. Modelling of Unmanned Aerial Vehicle Deliveries in Populated Urban Areas for Risk Management. *10th International Conference on Software, Knowledge, Information Management & Applications (SKIMA) Model* 2016; : 61–66.
5. Guglieri G, Quagliotti F and Ristorto G. Operational issues and assessment of risk for light UAVs. *Journal of Unmanned Vehicle Systems* 2014; 02(04): 119–129.
6. McGeer T. *Aerosonde hazard estimation*. The Insitu Group, Tech. Rep., 1994.
7. McGeer T, Newcome LR and Vagners J. Quantitative risk management as a regulatory approach to civil uavs. In *International Workshop on UAV Certification*. Paris, France, pp. 1–11.
8. Clothier R, Walker R, Fulton N et al. A casualty risk analysis for unmanned aerial system (UAS) operations over inhabited areas. *Second Australasian Unmanned Air Vehicle Conference* 2007; (March): 1–15.
9. Clothier RA and Walker RA. Determination and evaluation of uav safety objectives. In *21st International Unmanned Air Vehicle Systems Conference*. Bristol, United Kingdom, pp. 18.1–18.16.
10. Weibel R and Hansman RJ. An Integrated Approach to Evaluating Risk Mitigation Measures for UAV Operational Concepts in the NAS. *Infotech@Aerospace* 2005; (September): 509–519.

11. Lum CW, Gauksheim K, Deseure C et al. Assessing and Estimating Risk of Operating Unmanned Aerial Systems in Populated Areas. *American Institute of Aeronautics and Astronautics* 2011; (September): 1–13.
12. Frazzoli E, Dahleh MA and Eric F. Maneuver-based motion planning for nonlinear systems with symmetries. *IEEE Transactions on Robotics* 2005; 21(6): 1077–1091.
13. Etkin B. *Dynamics of Atmospheric Flight*. New York: John Wiley & Sons, 1972.
14. Foo JL, Knutzon J, Kalivarapu V et al. Path planning of unmanned aerial vehicles using b-splines and particle swarm optimization. *Journal of Aerospace Computing, Information, and Communication* 2009; 6(4): 271–290.
15. McCormick BW. *Aerodynamics, aeronautics, and flight mechanics*. New York: Wiley, 1995.
16. Avanzini G, Carlà A and Donateo T. Parametric analysis of a hybrid power system for rotorcraft emergency landing sequence. *Proceedings of the Institution of Mechanical Engineers, Part G: Journal of Aerospace Engineering* 2017; 231(12): 2282–2294.
17. Hixenbaugh AF. Fault tree for safety. Technical report, Boing Co. Seattle WA Support Systems Engineering, 1968.
18. Borgovini PSRM R. Failure mode, effects, and criticality analysis (fmeca). Technical report, Reliability Analysis Center, Griffiss AFB, NY., 1993.
19. Administration FA. *Flight Safety Analysis Handbook, Version 1.0*, chapter 6. Washington DC, USA: United States Department of Transportation, 2011. pp. 294–103.